JOURNAL OF THERMOPHYSICS AND HEAT TRANSFER
Vol. 11, No. 1, January–March 1997

Novel Approach for Calculating Equilibrium Radiating Flows

Frank J. Brauns* and H. A. Hassan†
North Carolina State University, Raleigh, North Carolina 27695

A two-dimensional/axisymmetric Navier–Stokes flow solver capable of handling hypersonic equilibrium radiating flows over aerobrake geometries of current interest is developed. Traditional computations of equilibrium flows use iterative schemes to enforce equilibrium at each time step. The present approach employs rate equations in lieu of expensive iterative procedures, with the result that equilibrium is achieved at convergence. Cases are presented, assuming both 5- and 11-species air models, highlighting important aspects of the method development. Results are shown for a proposed 15.2-m-diam lunar transfer vehicle with a velocity of 9797 m/s at 72 km altitude. The results are compared with those generated by the LAURA code.

Nomenclature

B = Planck function
b = shape factor
C = concentration
C_v = constant volume specific heat
$\hat{C}_v$ = effective constant volume specific heat
c = speed of light
e = internal energy or electron charge
$\boldsymbol{F}$ = vector of fluxes in the x direction
f = oscillator strength of a line
$\boldsymbol{G}$ = vector of fluxes in the y direction
H = total enthalpy
I = radiative intensity
J = emission coefficient
K_C = concentration equilibrium constant
M = molecular weight
m = electron mass
N = number density
q = heat flux
S = arc length
T = temperature
t = time or dummy variable of integration
$\boldsymbol{U}$ = vector of conserved variables
u = axial velocity
v = vertical velocity
$\boldsymbol{W}$ = vector of source terms
x = axial distance
Y = mass fraction
y = radial or vertical distance
Δh_f° = heat of formation at T_{ref}
η = body-normal coordinate
$\boldsymbol{\theta}$ = spherical coordinate
κ = relaxation factor
μ = absorption coefficient
ν = photon frequency
$\boldsymbol{\rho}$ = density
σ = cross section
τ = stress tensor
$\boldsymbol{\phi}$ = spherical coordinate

Subscripts
i = species i
j = absorbing level j
k = line k
r = radiative value
ref = reference value
s = species index
w = wall value
ν = spectral quantity
∞ = freestream values

Superscripts
C = continuum quantity
L = line property
r = 0 for two dimensional, 1 for axisymmetric
$+$ = downward directed intensity
$-$ = upward directed intensity

Introduction

INTEREST in pursuing a mission to Mars and lunar missions has spurred research into aerobraking as an efficient means of slowing down re-entry vehicles. Because of the harsh flow environment associated with re-entry flows, an aerobrake not only serves as a lifting and braking body, but also as a thermal protection system. A strong bow shock results in temperatures high enough to cause dissociation and ionization of the chemical species present. High convective heating rates and radiative emissions are also characteristic of these high-temperature flows. The radiative emissions may contribute significantly to the total heat flux incident on the vehicle surface. Thus, efficient design of an aerobraking system requires codes that are able to accurately predict both convective and radiative heat transfer.

Convenience has dictated the use of nonequilibrium Navier–Stokes solvers to calculate equilibrium flows. There are at least two conceptual difficulties associated with such an approach. The first pertains to the speed of sound; the equilibrium speed of sound is quite different from the frozen speed of sound appropriate for nonequilibrium flows. The difference between the equilibrium and frozen speeds of sound in air can be as high as 20%.[1] Second, standard practice is to artificially increase reaction rates to simulate equilibrium conditions. The net effect of increasing rate coefficients is to approach a condition corresponding to the steady-state approximation rather than to an equilibrium condition. In addition to the conceptual problems, there is the additional cost of integrating equations that describe thermal nonequilibrium. When radiation is considered, uncertainty in the proper modeling of the nonequilibrium excitation rates introduces questions about the accuracy

Received April 26, 1996; presented as Paper 96-1887 at the AIAA 31st Thermophysics Conference, New Orleans, LA, June 17–20, 1996; revision received July 25, 1996; accepted for publication July 25, 1996.

*Research Assistant, Mechanical and Aerospace Engineering Department, Campus Box 7910. Student Member AIAA.

†Professor, Mechanical and Aerospace Engineering Department, Campus Box 7910. Associate Fellow AIAA.

of the results. Formulation of a proper model for nonequilibrium radiation calculations is still a state-of-the-art research problem. Therefore, there is a need to develop an equilibrium flow solver that removes much of the uncertainties and needless work.

At present, the HYVIS[2] code is an efficient method for the calculation of radiative equilibrium flows, however, it uses the viscous shock layer (VSL) approximation and has difficulty with the very blunt body geometries under present consideration. This difficulty arises because the subsonic region for these vehicles is not constrained to the nose region, but can cover the whole forebody. A Navier–Stokes solver is not limited by such geometric constraints.

The present method is therefore designed to fill the computational void left by the aforementioned codes. The method involves the solution of the Navier–Stokes equations under the assumptions of thermochemical and radiative equilibrium. Equilibrium thermochemistry is well understood, thus eliminating many of the uncertainties involved with multiple temperature nonequilibrium formulations.

Physical Modeling and Computational Method

Solution of the equations governing radiating flows in thermochemical equilibrium involves separate determination of how to model the equilibrium chemistry, the flow, and the radiation. The approach used in this work was to develop a novel method for the solution of the equilibrium chemistry and to couple the method to standard flow and radiation solvers. As such, discussion of the physical modeling of the method starts with the chemical equilibrium formulation. A description of the important aspects of the flow and radiation solvers follows.

The present formulation is developed for entry flows in air. A standard 11-species air model is assumed to be valid. This involves the species, N_2, O_2, NO, N, O, NO^+, N_2^+, O_2^+, N^+, O^+, and e^-. With the elemental concentrations of N and O fixed, the equilibrium state is defined by any two independent thermodynamic variables. Generally, this is done by obtaining the pressure and temperature, and then applying a Gibbs free energy minimization technique[3,4] or an equilibrium constant method.[5] Since flow solvers generally return values for the conserved variables, ρ and ρE, applying these methods results in a computationally costly iterative procedure to couple the chemistry with the flow. One of the objectives of the new approach is to remove this costly iteration. The previous approaches incur additional expense by requiring equilibrium conditions to be maintained during the transient phase of the solution. Since the solver is integrated to a steady state, this is both physically and computationally unnecessary. Thus, the present method also focuses on removing this iteration.

The current approach builds on the use of an equilibrium constant method. A brief example can best describe the approach. Consider the formation of NO in an equilibrium situation. A reaction producing NO can be written as

$$\tfrac{1}{2}\mathrm{N_2} + \tfrac{1}{2}\mathrm{O_2} \rightleftharpoons \mathrm{NO} \tag{1}$$

The concentration, in moles per volume, at equilibrium is determined from

$$K_C = C_{\mathrm{NO}}/C_{\mathrm{O_2}}^{1/2} C_{\mathrm{N_2}}^{1/2} \tag{2}$$

The equilibrium constants are known functions of temperature. In traditional calculations, Eq. (2) would be solved at each grid point and each time step by an iterative procedure. Rather than follow this approach, the same result can be attained by replacing Eq. (2) by

$$\frac{\mathrm{d}C_{\mathrm{NO}}}{\mathrm{d}t} = \kappa(C_{\mathrm{N_2}}^{1/2} C_{\mathrm{O_2}}^{1/2} - K_C^{-1} C_{\mathrm{NO}}) \tag{3}$$

and integrating in time to a steady state. For convenience, the rate equation is actually integrated in terms of mass fractions, such that when

$$\frac{\mathrm{d}Y_{\mathrm{NO}}}{\mathrm{d}t} = \kappa \frac{M_{\mathrm{NO}}}{\rho}(C_{\mathrm{N_2}}^{1/2} C_{\mathrm{O_2}}^{1/2} - K_C^{-1} C_{\mathrm{NO}}) \tag{4}$$

reaches steady-state conditions, Eq. (2), which must hold for equilibrium concentrations, is satisfied. In this form, the previous equation can be integrated in time along with the flow equations. This eliminates the unnecessary iteration enforcing the equilibrium condition at each time step.

The previous method is applied to the 11 species currently under consideration. Since there are 11 unknown species concentrations, there must be 11 equations to solve for those unknowns. In this case, eight independent reactions can be written as

$$\tfrac{1}{2}\mathrm{N_2} + \tfrac{1}{2}\mathrm{O_2} \rightleftharpoons \mathrm{NO}, \qquad \tfrac{1}{2}\mathrm{N_2} \rightleftharpoons \mathrm{N}, \qquad \tfrac{1}{2}\mathrm{O_2} \rightleftharpoons \mathrm{O}$$

$$\tfrac{1}{2}\mathrm{N_2} + \tfrac{1}{2}\mathrm{O_2} \rightleftharpoons \mathrm{NO^+} + \mathrm{e^-}, \qquad \mathrm{N_2} \rightleftharpoons \mathrm{N_2^+} + \mathrm{e^-}$$

$$\mathrm{O_2} \rightleftharpoons \mathrm{O_2^+} + \mathrm{e^-}, \qquad \tfrac{1}{2}\mathrm{N_2} \rightleftharpoons \mathrm{N^+} + \mathrm{e^-}, \qquad \tfrac{1}{2}\mathrm{O_2} \rightleftharpoons \mathrm{O^+} + \mathrm{e^-}$$

from which eight rate equations of the form of Eq. (4) are found. The three remaining equations are two equations conserving elemental nitrogen and elemental oxygen and a conservation of charge equation forcing the number of electrons to equal the number of ions. The conservation statements are algebraic expressions that can be directly substituted into the rate expressions. Thus, for the 11-species model, it is necessary to carry out the integration on only eight species equations.

The next objective is to remove the iterative procedure necessary for the coupling of the flow equations to the chemistry. Recall that flow solvers return values for ρ and the internal energy ρE, and that the equilibrium composition is found through knowledge of the temperature and pressure in a system. However, with the previous formulation, the composition at each time step is known along with ρ and ρE. Therefore, it is only necessary to now find the temperature and pressure. This is accomplished without iteration in the following manner. First, consider the definition for the internal energy of a species mixture:

$$e = \sum_{s=1}^{nsp} Y_s \left(\int_{T_{\mathrm{ref}}}^{T} C_{v,s}\, \mathrm{d}T + \Delta h_{f,s}^{\circ} \right) \tag{5}$$

An effective specific heat is defined so that

$$\int_{T_{\mathrm{ref}}}^{T} C_{v,s}\, \mathrm{d}T = \hat{C}_{v,s} T \tag{6}$$

The integral of the specific heat can be evaluated through the polynomial curve fits of Gupta et al.,[6] with the temperature lagged from the previous iteration. Since e can be found readily from ρE, the temperature can just be evaluated by the expression

$$T = \left(e - \sum_{s=1}^{nsp} Y_s \Delta h_{f,s}^{\circ} \right) \Bigg/ \left(\sum_{s=1}^{nsp} Y_s \hat{C}_{v,s} \right) \tag{7}$$

Dalton's law is used to obtain the pressure of the system.

With the chemistry thus determined, integration of the flow equations is examined. The two-dimensional/axisymmetric Navier–Stokes equations are written in conservation law vector form as

$$\frac{\partial U}{\partial t} + \frac{\partial}{\partial x} \boldsymbol{F}(\boldsymbol{U}) + \frac{1}{y^r} \left[\frac{\partial}{\partial y} y^r \boldsymbol{G}(\boldsymbol{U}) \right] = \boldsymbol{W} \tag{8}$$

The convective fluxes, $\boldsymbol{F}$ and $\boldsymbol{G}$, can be considered as the sum of inviscid fluxes and viscous fluxes. The inviscid flux calculations are carried out using Roe's scheme because of its ability to capture shock waves and resolve the boundary-layer gradients with a minimum number of points.[7] Roe's scheme is extended to second order using the MUSCL approach.[8] The viscous fluxes are treated by standard central differencing in each direction. The equilibrium chemistry computation is coupled into the flow solution through the implicit time integration. The flow is integrated in time with the Gauss–Seidel line integration technique with implicit boundary conditions as described by Candler.[9] Additionally, a correction to the inviscid time linearization was added to take into account the viscous effects and improve propagation of viscous information.[10] The resulting matrix from the previous procedure is block tridiagonal. However, if the form of Eq. (4) is examined, it is seen that the time derivative term can be considered as part of $\boldsymbol{U}$, and the right-hand side as part of $\boldsymbol{W}$. Linearizing the equations again as done for the Gauss–Seidel technique now results in a block tridiagonal matrix for the flow equations coupled to a block diagonal matrix for the chemical equations.

The last modeling concern is the inclusion of equilibrium radiation into the solver. The radiation term appears in Eq. (8) in the evaluation of flux terms, $\boldsymbol{F}$ and $\boldsymbol{G}$, in the energy equation

$$\begin{aligned} \boldsymbol{F} &= \boldsymbol{\rho} u H - u\tau_{xx} - v\tau_{xy} + q_x + q_{rx} \\ \boldsymbol{G} &= \boldsymbol{\rho} v H - u\tau_{xy} - v\tau_{yy} + q_y + q_{ry} \end{aligned} \tag{9}$$

Notice that Eq. (8) actually involves the spatial derivatives of the flux terms. Thus, the information necessary from the radiation calculation is the radiative flux divergence term, $\nabla \cdot \boldsymbol{q}_R$. The radiation transport code, RADICAL,[11,12] is used in the present work for the calculation of this term. RADICAL applies the tangent slab approximation to simplify the calculation. This approximation assumes that the gas properties only change in the direction normal to the surface of the body. This is a good approximation for the stagnation region of the blunt bodies currently under consideration as aerobrakes. The effect of making this assumption is that the flux divergence term is reduced to $\nabla \cdot \boldsymbol{q}_R = \mathrm{d}q_R/\mathrm{d}\eta$. Details of the derivation of the tangent slab model can be found in Anderson.[1]

For equilibrium applications, the absorption coefficients provide all of the necessary information to carry out the radiation computation. This is because the emission coefficients can be directly related to the absorption coefficients through the Planck function, i.e., $J_\nu = \mu_\nu B_\nu$. The radiative intensity is generally integrated in terms of the optical thickness, $\tau_\nu = \int_0^L \mu_\nu \, \mathrm{d}S$, producing the following result for a downward directed ray:

$$I_\nu^+ = I_\nu^+(\tau_{\nu 2}) \exp\left[\frac{(\tau_{\nu 2} - \tau_\nu)}{\cos\theta}\right] + \int_{\tau_\nu}^{\tau_{\nu 2}} B_\nu(t) \exp\left[\frac{-(t - \tau_\nu)}{\cos\theta}\right] \frac{\mathrm{d}t}{\cos\theta} \tag{10}$$

I_ν^+ is then just a function of the optical depth, which is only a function of the absorption coefficient. With this known, the radiative heat flux in that direction, q^+ is

$$q^+ = \int_0^\infty \int_0^{2\pi} \int_0^{\pi/2} I_\nu^+ \cos\theta \sin\theta \, \mathrm{d}\theta \, \mathrm{d}\boldsymbol{\phi} \, \mathrm{d}\nu \tag{11}$$

where the integrals cover the full range of possible frequencies and radiative intensity directions in the downward direction. With a similar formula for the upward-directed flux, the total radiative flux at a given location is given as $q = q^+ + q^-$. An important point to emphasize is that when the absorption coefficients are determined, all of the information necessary for coupling to the flow equations is known. The radiation calculation is computationally expensive. Therefore, when coupled to the flow solver, the radiative heat flux divergence is only updated every 250–1000 flow iterations.

Since the evaluation of the absorption coefficients is the driving mechanism for determining the radiative heat flux, it is important to describe the methods applied to obtain the radiative absorption coefficients. The absorption coefficients are functions of temperature, density, and frequency, i.e., a nongray gas. The absorption coefficient at a given frequency can be written as the sum of the contributions from all continuum transitions and from all line transitions. In other words

$$\mu_\nu = \sum_{i=1}^{N_C} \mu_i^C(\nu) + \sum_{k=1}^{N_L} \mu_k^L(\nu) \tag{12}$$

RADICAL takes into account atomic continuum and molecular band transitions for the continuum contribution, and ionic and atomic line transitions for the contributions from the lines. The continuum transitions are discussed first.

Continuum transitions arise from photoionization, photodetachment, free–free transitions, and photodissociation. These transitions, in general, are just functions of the number density and cross section of the absorbing level. This is written as

$$\mu_i^C(\nu) = \sum_j N_{i,j} \sigma_{ij}^C(\nu) \tag{13}$$

The number densities are readily found from the thermodynamic data given by the flow solver. The cross sections are taken either from tabulated data[13] or are modifications to the hydrogen cross section. The other continuum mechanism concerns molecular band transitions. This is radiation originating from the closely spaced energy levels of molecules. The radiation from these levels can be considered as a continuum and are designated as band systems. To provide a continuous variation of the absorption coefficient, each band within the band system is smeared into what is termed a bandless model. The absorption coefficients for the molecular band transitions are found from curve fits to experimental data. The bands considered for air are the 1^+, 2^+, and Birge Hopfield systems for N_2, the Schumann–Runge system for O_2, the γ, $\boldsymbol{\beta}$, ε, and δ systems for NO, and the 1^- system for N_2^+.

The treatment of ionic and atomic line transitions is now examined. Again, the absorption coefficient is a function of the population of the absorbing level, but is now also a function of the line shape. Nicolet[11] writes this as

$$\mu_{k(j)}^L(\nu) = (\pi e^2/mc) f_{k(j)} N_{ij} b_{k(j)}(\nu, T, P, x_1, x_2, \ldots) \tag{14}$$

The line shape is a function of the frequency and the equilibrium state of the gas and must be considered because of broadening of the line via perturbations from electron impacts, known as Stark broadening, or to impacts with other atoms, known as resonance or collision broadening, or to the Doppler effect resulting from the random thermal motion of the molecules. Because of this, the lines can no longer be considered discrete values. Each line is thus resolved by about 15 spectral points. The line center is always one of the points to make sure the peak value is captured.

To reduce the computational effort of obtaining the radiative heat flux from all of the lines calculated, the line group approximation is employed. With this approximation, the range of frequencies considered is broken down into about 20 frequency increments, which are not necessarily contiguous. The contribution to the absorption coefficient is found by summing all of the contributions of the lines within each frequency increment. Thus, there remain only 20 absorption coefficients to work with as opposed to one for each individual line considered. Since the optical depth, as shown earlier, is an integral

function of the absorption coefficient, the line grouping approximation represents a significant reduction in the amount of work required to obtain a solution.

Some of the lines are not treated with the previous line grouping technique, but are treated as a continuum. The method assumes the high series lines, those associated with transitions with lower levels that have a high principal quantum number (≥ 4), can be treated as a continuum contribution. This is because the energy levels get more closely spaced as the principal quantum number increases. The high lines are also included with the continuum contributions. These are the transitions that have their upper levels with large principal quantum numbers. RADICAL accounts for these transitions by treating them as if they were continuum photoionization processes by lowering the photoionization limit.

Results and Discussion

Four cases will be presented to describe the behavior of the new approach. The first three are developmental cases highlighting important aspects of the method behavior. The last is a case of current practical interest; the re-entry of a lunar transfer vehicle (LTV). Except for changes in the freestream Mach number, the same freestream conditions were employed for each case to be that of the LTV case. The case conditions are taken from Gnoffo[14] for an altitude of 72 km, which results in $T_\infty = 213.7$ K, $\rho_\infty = 5.987 \times 10^{-5}$ kg/m^3. Three cases are run at increasing velocities to test the behavior of the method, $V_\infty = 1758.4$, 4689.0, and 9797.0 m/s corresponding to Mach numbers of 6.0, 16.0, and 33.4, with the highest velocity case being the one run by Gnoffo et al.[14] To validate that the proper equilibrium mass fractions are found by the present method, comparisons are made by taking the temperature and pressure from the converged solution and applying the Gibbs energy minimization technique.

Initial testing of the method was done on a sphere of radius 1 m in a Mach 6 freestream flow considering only a five-species air model, which includes N_2, O_2, NO, N, and O. The code converged five orders of magnitude in 3000 iterations, which took approximately 12 min of Cray Y-MP time. Figure 1 shows smooth temperature contours and Fig. 2 shows that the mass fractions have converged to the values given by the Gibbs energy minimization method. The flat region for the composition of N is a result of setting a minimum value of 10^{-15} for the species mass fractions. Since the mass fractions of NO, N, and O are still rather insignificant for this case, this case only demonstrates the viability of the method.

Applying the method to higher Mach number cases results in higher shock layer temperatures and, thus, changes in chemistry become significant. The next case is applied at Mach 16 with the geometry of the LTV used instead of the sphere. Again, only five species are considered. The code was converged five orders of magnitude in 16,000 iterations. The extra iterations are a reflection on the time required to relax the chemistry to the equilibrium values. In addition, extra expense may be a result of the sensitivity of the shock shape to the larger elliptic subsonic region for this geometry. Figures 3 and 4 show that it again produces smooth contours and that the mass fractions have converged to the equilibrium values. Additionally, some adjustment to κ was found to be necessary to improve convergence. κ was initially set to 50, however, it was seen that NO was converging to the equilibrium value at a much slower rate than either N or O. Thus, an additional factor of 50 was multiplied times the original κ for that reaction. Since the rate equations at steady state produce the equilibrium condition regardless of the value of κ, such adjustments can be made without harm to the final solution. However, to keep the model as simple as possible, only the base value and one multiplier are ever used to speed up any reactions.

The next case upgraded from 5 to the 11-species air model. This was done because any practical case involving the re-

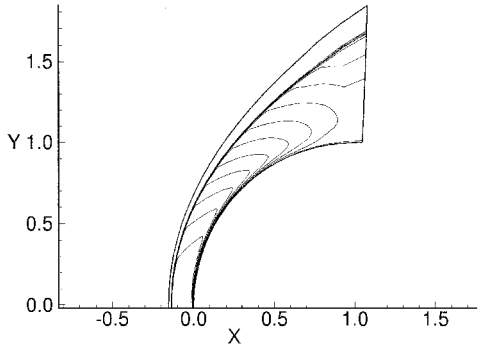

Fig. 1 Temperature contours for a Mach 6 flow about a sphere (five species).

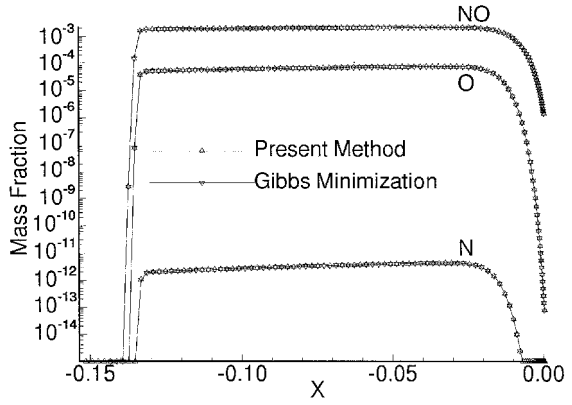

Fig. 2 Stagnation line mass fractions for Mach 6 flow about a sphere.

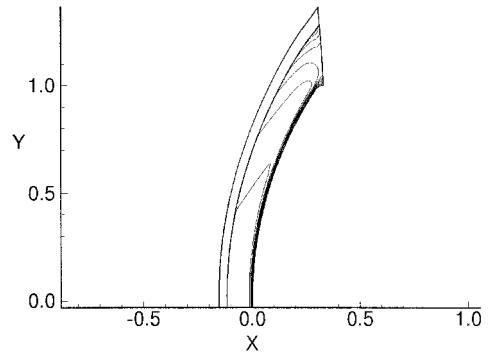

Fig. 3 Temperature contours for a Mach 16 flow about an LTV (five species).

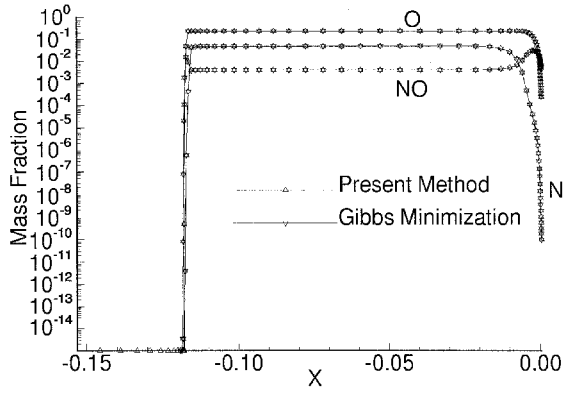

Fig. 4 Stagnation line mass fractions for Mach 16 flow about an LTV (five species).

entry of an LTV would have to take into account the ionized species. Testing was done again at Mach 16. The addition of the extra species resulted in an increase in the number of iterations required for convergence from 16,000 to 24,000, and an increase in computational time on a Cray Y-MP from 1 to 2 h 50 min. Much of this cost can be attributed to the solution of the larger matrices associated with the extra species equations. Similar results are seen for the temperature contours in Fig. 5 as the previous case, since the mass fractions of the ionized species are still negligible (see Fig. 6). It was necessary to multiply κ by 50 for both NO and NO^+. These values are the same as those used for the final case.

The last case has been computed for comparison with the Langley aerothermodynamic upwind relaxation algorithm (LAURA). The case is for a proposed LTV at 72 km altitude with a freestream velocity of 9797 m/s.[14] The LTV is a 15.2-m-diam vehicle composed of a 13.6-m-radius spherical segment and a 0.3048-m-radius shoulder. Figure 7 shows the geometry of the vehicle and a sample grid used for the calculation. Only every other grid point in the surface normal direction is shown for clarity. The grid adaption procedure of Gnoffo[14] was used to obtain the grid clustering. Gnoffo[14] also performed an extensive grid convergence study for this case. It was deemed sufficient to use only 64 surface normal points when the grid adaption was applied. The current study uses 91 points in the surface normal direction with the same clustering parameters described by Gnoffo et al.[14] for the adaption to ensure adequate grid resolution. This case was chosen for comparison because the LAURA results show it is nearly in full equilibrium.

This case is a good test of the abilities of the present method to calculate equilibrium flows. First, the high velocity will produce a strong shock, which will dissociate almost all of the N_2 and O_2 present in the system. A significant amount of ionization will also occur. We thus have a case in which the mass fractions through the shock layer vary widely from the freestream mass fractions for all species present. The extremity of the conditions had an adverse affect on the convergence of the method, however. This case took over 250,000 iterations to converge. Because of the changes in chemistry with shock movement, it became difficult to use the density residual as a marker for convergence. Instead, convergence was taken when the heat transfer rate reached a steady state and the equilibrium compositions were those satisfied by the Gibbs energy minimization method. Since these cases are initial tests of the new method, the number of iterations required for computations is expected to decrease after optimization of the parameters used in the computation. These parameters include choosing an optimal κ to increase the speed of the reactions without affecting the stability of the solver and applying the grid adaption routine in a more efficient manner.

Comparisons are shown for the chemical composition obtained from the LAURA code versus those with the present method. Figures 8–10 show the mass fractions of the most significant species through the shock layer. N and O become the most dominant species, with N^+ and O^+ being the most significant ionized species. Also of note is that N_2 completely recombines at the wall.

Comparisons of some of the convective flow parameters are now given. Figure 11 shows the relative shock positions calculated by each method. The shock location shown is the first point at which the temperature reaches 1000 K. The temperature used from the LAURA calculation is the translational temperature. Stagnation line results are shown for the LAURA code vs the present method using the translational temperature from LAURA and the present method equilibrium temperature in Fig. 12. What this figure demonstrates is the region of nonequilibrium taken into account in the LAURA code at the shock. The present method, which produces strictly equilibrium results, defines a much sharper shock and demonstrates

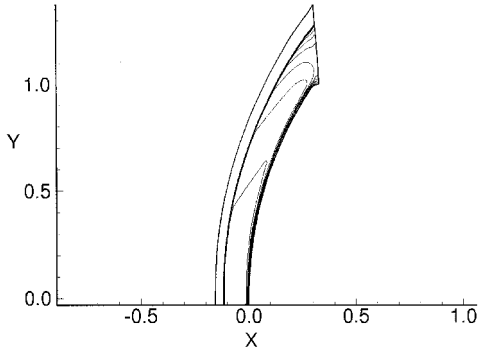

Fig. 5 Temperature contours for Mach 16 flow about an LTV (11 species).

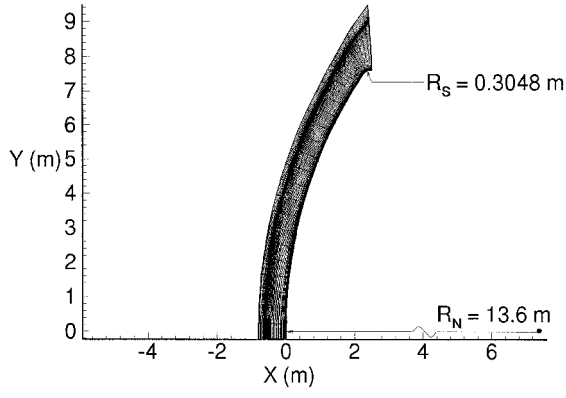

Fig. 7 Geometry of the LTV and final computational mesh (31 × 91).

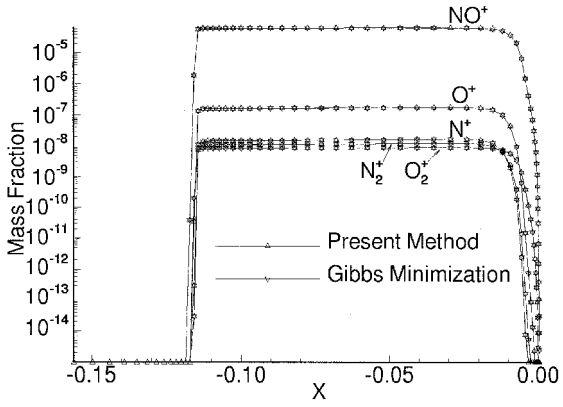

Fig. 6 Stagnation line mass fractions for Mach 16 flow about an LTV (11 species).

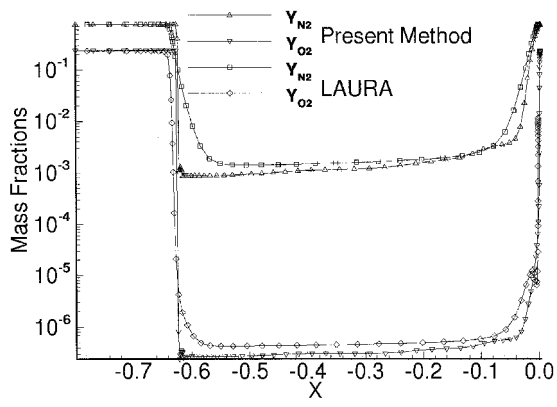

Fig. 8 Comparison of stagnation line mass fractions of N_2 and O_2 (LTV).

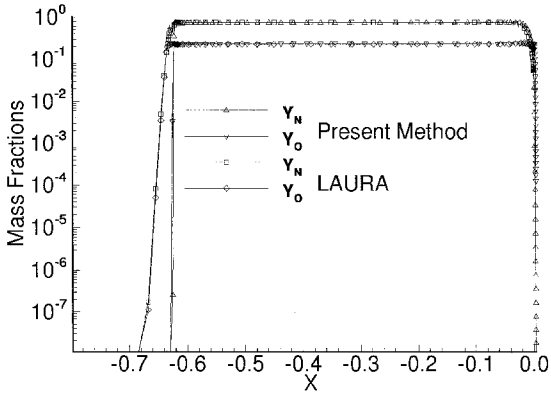

Fig. 9 Comparison of stagnation line mass fractions of N and O (LTV).

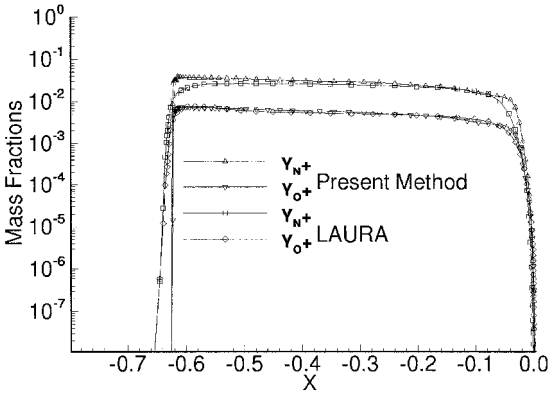

Fig. 10 Comparison of stagnation line mass fractions of N^+ and O^+ (LTV).

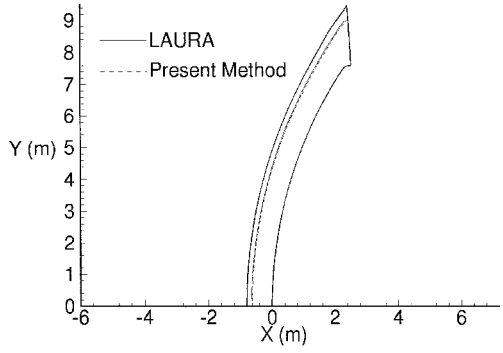

Fig. 11 Shock location comparison (LTV).

no overshoot in temperature, as is typical for nonequilibrium methods. LAURA indicates a short region of nonequilibrium around the shock that relaxes into equilibrium just downstream of the shock. Once past this zone of nonequilibrium, there is good agreement between the two methods in predicting the equilibrium flow through the shock layer.

What is really of importance for these flows, however, is the prediction of the heating rates. Figure 13 shows the predictions of convective heating for this body. The present method predicts higher convective heating along the surface of the body. This is consistent with previous comparisons to the LAURA code.[15] The heating curve shows the same trend along the whole surface. The larger spike in the shoulder heating is a result of the sensitivity of the solution to the grid resolution in that area and the differences in chemical composition in the boundary layer at that point for the two methods. Figure 14 shows the radiative heating curves predicted by the present method and LAURA. The two extra data points

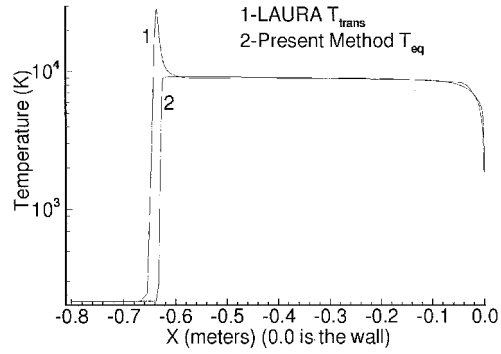

Fig. 12 Stagnation line LAURA T_{trans} vs present method T_{eq}.

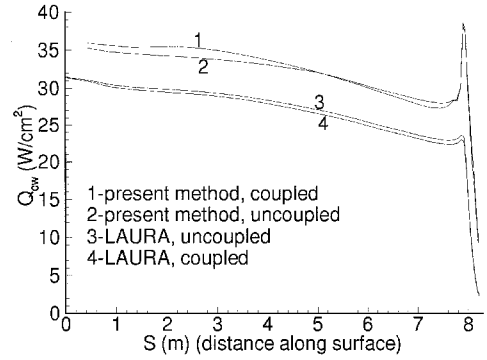

Fig. 13 Coupled and uncoupled convective heating.

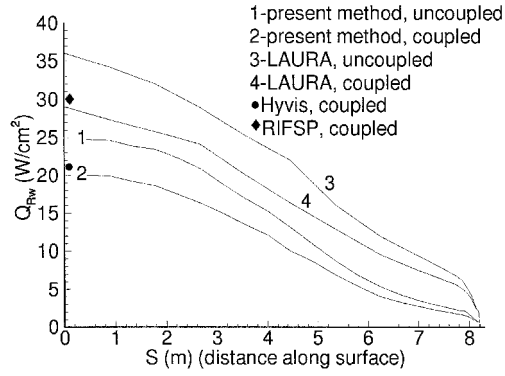

Fig. 14 Coupled and uncoupled radiative heating.

are the stagnation point radiative heating values from the HYVIS code and from Sutton's RIFSP code,[16] an inviscid stagnation line code with coupled radiation. Both of these codes also apply the RADICAL code for the calculation of the radiative heat flux. It is readily seen that, as expected, the uncoupled radiation cases provide higher heating rates to the body than the coupled case. This is because of the radiative cooling of the shock layer by the radiative emissions. In this case, the LAURA results show that q_{Rw} is higher than that predicted by the present method. This is, in part, because much of the radiation being attributed to the higher temperatures present in the nonequilibrium shock.[14] The LAURA results for coupled radiation appear close to that given by Sutton's inviscid code. The present method results for coupled radiative heating are close to that given by the HYVIS code. This is to be expected since the inviscid results will be higher because of the lack of an absorbing boundary layer.[17]

Some points to note are the differences between the radiation solvers used for the previous comparisons. These may also be a factor in the differences in the level of radiative heating calculated by the flow solvers. The LAURA code results shown employ the LORAN.[18] The prime difference is that

LORAN deals with nonequilibrium radiation, which requires various excitation rates that are not well known. Moreover, the number densities of the various excited states are determined by using a steady-state approximation. This may be contrasted with the present approach where equilibrium conditions determine a unique relation between absorption and emission and determine the number densities of the excited states.

Concluding Remarks

The results shown indicate that reasonable agreement exists between the solutions of the present method and that provided by the LAURA code. Also, good agreement exists in the stagnation radiative heating data of the present method compared to the HYVIS results. It should be noted that the differences in the heating curves between the present method and the LAURA code can be attributed to the small nonequilibrium region near the shock from the LAURA results. Comparisons of the mass fractions through the shock layer show that equilibrium results are obtained by the present method without having to enforce an equilibrium state through the computationally expensive Gibbs energy minimization iteration. Some concerns are brought on by the number of iterations required for convergence of the method in extreme cases. This can be greatly alleviated by incorporating a shock-fitting technique.

Acknowledgments

This work was supported in part by NASA's Cooperative Agreement NCCI-112 and the Mars Mission Research Center, funded by NASA Grant NAGW-1331. The authors would also like to thank the North Carolina Supercomputing Center for the use of their resources. Personal thanks go to Ken Sutton, Peter Gnoffo, Lin Hartung Chambers, and Roop Gupta of the NASA Langley Research Center, and also to David Olynick of the NASA Ames Research Center, Jeff Taylor of Johns Hopkins Applied Physics Laboratory, and Jay Edwards of North Carolina State University for their help in completing the project.

References

[1]Anderson, J. D., Jr., *Hypersonic and High Temperature Gas Dynamics*, McGraw–Hill, New York, 1989, Chaps. 14, 18.

[2]Moss, J. N., "Reacting Viscous-Shock-Layer Solutions with Multicomponent Diffusion and Mass Injection," NASA TR R-411, June 1974.

[3]White, W. B., Johnson, S. M., and Dantzig, G. B., "Chemical Equilibrium in Complex Mixtures," *Journal of Chemistry and Physics*, Vol. 28, No. 5, 1958, pp. 751–755.

[4]Stroud, C. W., and Brinkley, K. L., "Chemical Equilibrium of Ablation Materials Including Condensed Species," NASA TN D-5391, Aug. 1969.

[5]Kuo, K. K., *Principles of Combustion*, Wiley, New York, 1986, Chap. 1.

[6]Gupta, R. N., Yos, J. M., Thompson, R. A., and Lee, K. P., "A Review of Reaction Rates and Thermodynamic and Transport Properties for an Eleven-Species Air Model for Chemical and Thermal Nonequilibrium Calculations to 30000K," NASA RP-1232, Aug. 1990.

[7]Van Leer, B., Thomas, J. L., Roe, P. L., and Newsome, R. W., "A Comparison of Numerical Flux Formulas for the Euler and Navier-Stokes Equations," AIAA Paper 87-1104, June 1987.

[8]Van Leer, B., "Towards the Ultimate Conservation Difference Scheme. V. A Second Order Sequel to Godunov's Method," *Journal of Computational Physics*, Vol. 32, No. 1, 1979, pp. 101–136.

[9]Candler, G. V., "Computation of Weakly Ionized Hypersonic Flows in Thermo-Chemical Nonequilibrium," Ph.D. Dissertation, Stanford Univ., Stanford, CA, June 1988.

[10]Tysinger, T. L., and Caughey, D. A., "Implicit Multigrid Algorithm for the Navier-Stokes Equations," AIAA Paper 91-0242, Jan. 1991.

[11]Nicolet, W. E., "Advanced Methods for Calculating Radiation Transport in Ablation-Product Contaminated Boundary Layers," NASA CR-1656, Sept. 1970.

[12]Nicolet, W. E., "Rapid Methods for Calculating Radiation Transport in the Entry Environment," NASA CR-2528, April 1975.

[13]Wilson, K. H., and Nicolet, W. E., "Spectral Absorption Coefficients of Carbon, Nitrogen and Oxygen Atoms," *Journal of Quantitative Spectroscopy and Radiative Transfer*, Vol. 7, No. 6, 1967, pp. 891–941.

[14]Gnoffo, P. A., Hartung, L. C., and Greendyke, R. B., "Heating Analysis for a Lunar Transfer Vehicle at Near-Equilibrium Flow Conditions," AIAA Paper 93-0270, Jan. 1993.

[15]Olynick, D. R., "A New LU-SGS Flow Solver for Calculating Reentry Flows," Ph.D. Dissertation, Dept. of Mechanical and Aerospace Engineering, North Carolina State Univ., Raleigh, NC, 1992.

[16]Sutton, K., "Characteristics of Coupled Nongray Radiating Gas Flows with Ablation Products Effects About Blunt Bodies During Planetary Entries," Ph.D. Dissertation, North Carolina State Univ., Raleigh, NC, 1973.

[17]Gupta, R. N., Lee, K. P., Moss, J. N., and Sutton, K., "A Viscous-Shock-Layer Analysis of the Martian Aerothermal Environment," AIAA Paper 91-1345, June 1991.

[18]Hartung, L. C., "Development of a Nonequilibrium Radiative Heating Prediction Method for Coupled Flowfield Solutions," *Journal of Thermophysics and Heat Transfer*, Vol. 6, No. 4, 1992, pp. 618–625.